ELSEVIER

Computers & Geosciences 32 (2006) 109–123

COMPUTERS & GEOSCIENCES

www.elsevier.com/locate/cageo

SUA: A computer program to compute regolith site-response and estimate uncertainty for probabilistic seismic hazard analyses ☆

David Robinson*, Trevor Dhu, John Schneider

Risk Research Group, Geospatial and Earth Monitoring Division, Geoscience Australia, GPO Box 378, Canberra ACT 2601, Australia

Received 25 November 2003; received in revised form 23 February 2005; accepted 23 February 2005

Abstract

The presence of soils, geological sediments and weathered rock (collectively known as regolith) can amplify the level of ground shaking experienced during an earthquake. Consequently, including the affect of regolith on earthquake ground shaking is an important component of any seismic hazard analysis. This manuscript provides a detailed and comprehensive description of equivalent linear site-response analysis, a technique for modelling the amplification of seismic waves due to propagation through regolith. The description includes a theoretical solution of the wave equation, derivation of a transfer function relating bedrock acceleration to surface acceleration, calculation of a response spectral acceleration and computation of an amplification factor.

This paper also presents a simple approach for estimating the level of uncertainty in the modelled amplification factors due to variations in regolith thickness and velocity structure. A suite of MATLAB routines referred to as SUA are provided to implement an equivalent linear site-response analysis with the option of including an assessment of uncertainty. An example from Sydney, Australia demonstrates the techniques ability to successfully estimate site-response and associated uncertainties.

Keywords: Equivalent linear site-response; Regolith; Uncertainty; Amplification factor; Response spectral acceleration

1. Introduction

Earthquake hazard is typically quantified in terms of the level of ground shaking that has a certain chance of being exceeded in a given time period. The characterisation of earthquake hazard is of fundamental importance for defensive engineering design and is essential when modelling earthquake risk, where risk is defined as the likelihood that a social or economic consequence will be suffered (McGuire and Arabasz, 1990). A Probabilistic Seismic Hazard Analysis (PSHA) provides a framework for which uncertainty in the size, location and likelihood of future earthquakes can be incorporated to model earthquake hazard. For example, earthquake hazard estimates from the United States Geological Survey National Hazard Maps (Frankel et al., 2000) as well as recent estimates of earthquake hazard for New Zealand (Stirling and Wesnousky, 1998) are modelled using a PSHA.

☆Code available from server at http://www.iamg.org/CGEditor/index.htm.

*Corresponding author. Tel.: +61 2 6249 9156; fax. +61 2 6249 9986.

E-mail addresses: david.robinson@ga.gov.au, david.robinson@anu.edu.au (D. Robinson).

0098-3004/$ - see front matter Crown Copyright © 2005 Published by Elsevier Ltd. All rights reserved.
doi:10.1016/j.cageo.2005.02.017

The presence of regolith, where regolith is defined as the geological sediments and weathered rock that overly the unweathered bedrock, can increase the level of ground shaking experienced during an earthquake (Borecherdt and Gibbs, 1976; Murphy et al., 1971). For example, studies in the San Fernando Valley and Los Angeles Basin, USA have demonstrated that the damage patterns observed during the 1994 Northridge, California earthquake can be strongly correlated to site-response of local regolith (Meremonte et al., 1996). The consideration of how earthquake hazard is affected by the presence of regolith is a vital component of any PSHA.

Modelling the effect of regolith on earthquake ground shaking is commonly referred to as regolith site-response modelling. One of the most widely accepted techniques for regolith site-response modelling involves the use of an equivalent linear approach to solve the wave equation describing vertically propagating shear waves. There are numerous publications describing components of equivalent linear site-response analysis. However, to the best of the authors knowledge there are no comprehensive descriptions of the entire process of an equivalent linear site-response analyses describing the:

- equivalent linear solution of the wave equation (Seed and Idriss, 1970; Kramer, 1996; Bardet, et al., 2000; Idriss and Sun, 1992);
- calculation of response spectral acceleration (Chopra, 2001; FEMA,1999) and;
- modelling of the regolith site-response in terms of an amplification factor (Dhu and Jones, 2002; Silva et al., 1988).

This manuscript provides a detailed theoretical discussion of the equivalent linear site-response analysis. In addition, the paper presents a simple approach for estimating uncertainties in site-response studies that arise from the random variability inherent in the Earth and natural processes. Such estimates of uncertainty are required to obtain more realistic models of earthquake hazard (Annaka and Yashiro, 2000; Cramer et al., 1996). A case study from Botany Bay, Sydney, Australia is presented to demonstrate the application of SUA to a specific regolith site-response problem.

2. Equivalent linear regolith site-response analysis

The primary cause of amplification of earthquake motion is the decrease in velocity of seismic waves in regolith relative to the underlying bedrock. The decrease in velocity coupled with the conservation of energy leads to an increase in the amplitude of the ground shaking. Furthermore, the contrast between the regolith and underlying bedrock causes a series of reflections that generate upward and downward travelling waves. The interference of these waves modifies the ground shaking observed at any location.

Most seismic waves propagate through the regolith in a non-linear manner. That is, regolith material properties such as shear modulus and damping are themselves dependent on the level of earthquake energy. Site-response analyses that consider this non-linearity by solving the non-linear wave equation require a detailed knowledge of the regolith that is often beyond the scope of broad scale geotechnical studies. In contrast, an equivalent linear site-response analysis overcomes the problem of non-linearity by assuming that the critical regolith parameters are linear over a finite range of strain. An iterative approach is used to determine parameters that are compatible with the linear wave equation for the level of strain induced by the earthquake of interest. The equivalent linear solution of the wave equation was first introduced by Seed and Idriss (1970) and is an example of the general equivalent linear theory introduced by Iwan (1967).

2.1. Wave equation

The site-response analysis described hereafter involves numerically modelling the vertical propagation of seismic shear waves through a simplified horizontally layered model of regolith. Approximately 75% of the power associated with ground shaking observed at the surface of a regolith profile can be attributed to vertically propagating shear waves (EPRI, 1993). Horizontal shaking is also the primary cause of damage during most earthquakes since buildings and other structures are considerably more vulnerable to horizontal motion. Silva (1997) states how the horizontal shaking associated with earthquakes can be modelled with vertically propagating shear waves.

The one-dimensional wave equation for a vertically propagating shear wave in an elastic medium is

$$\rho \frac{\partial^2 u(z,t)}{\partial t^2} = \frac{\partial \tau}{\partial z}, \tag{1}$$

where ρ represents the density of the medium, τ the vertically directed shear stress, u the particle displacement, and z and t the depth and time of observation respectively (Kramer, 1996). The Earth can be approximated by a Kelvin–Voigt solid, a particular class of elastic solid, when considering the propagation of seismic waves. Bardet et al. (2000) state that the stress–strain relationship for a Kelvin–Voigt solid in shear can be expressed by

$$\tau(z,t) = G\gamma(z,t) + \eta \frac{\partial \gamma(z,t)}{\partial t}, \tag{2}$$

where G represents the shear modulus of the material, η the equivalent viscosity and γ the strain given by

$$\gamma(z,t) = \frac{\partial u(z,t)}{\partial z}. \tag{3}$$

Using Eqs. (1)–(3) the one-dimensional wave equation for a vertically propagating shear wave in a Kelvin-Voigt solid is given as

$$\rho \frac{\partial^2 u(z,t)}{\partial t^2} = G \frac{\partial^2 u(z,t)}{\partial z^2} + \eta \frac{\partial^3 u(z,t)}{\partial z^2 \partial t}. \tag{4}$$

Vertically propagating shear waves can be represented by the infinite sum of simple harmonic waves (Cramer et al., 1996). For a simple harmonic wave with circular frequency ω, the solution to Eq. (4) can be separated into a time-dependant component $e^{i\omega t}$ and a depth dependent component $U(z)$

$$u(z,t) = U(z)e^{i\omega t}. \tag{5}$$

Substituting Eq. (5) into Eq. (4) and simplifying yields the second order ordinary differential equation

$$G^* \frac{d^2 U}{dz^2} = -\rho\omega^2 U, \tag{6}$$

where

$$G^* = G + i\omega\eta \tag{7}$$

is the complex shear modulus. It is convenient to express G^* in terms of a damping ratio, ξ, as follows:

$$G^* = G(1 + 2i\xi), \tag{8}$$

where the relationship between equivalent viscosity and the damping ratio is

$$\omega\eta = 2G\xi \tag{9}$$

(Schnabel et al., 1972). Assuming that ρ, G and ξ are independent of U and its partial derivatives, t and z, then Eq. (6) is linear and has solution of form

$$U(z) = Be^{ik^* z} + Ce^{-ik^* z}, \tag{10}$$

where B and C are the amplitudes of upward and downward travelling waves respectively and k^* is the complex wave number given by

$$k^* = \omega\sqrt{\frac{\rho}{G^*}}. \tag{11}$$

Substituting Eq. (10) into Eq. (5) gives

$$u(z,t) = Be^{i(\omega t + k^* z)} + Ce^{i(\omega t - k^* z)}, \tag{12}$$

which is a solution to Eq. (4) for a simple (or single) harmonic wave. Note that the generalised solution to Eq. (4) is given by

$$u(z,t) = \sum_{n=-\infty}^{\infty} u^{(n)}(z,t), \tag{13}$$

where

$$u^{(n)}(z,t) = B_n e^{i(\omega_n t + k^* z)} + C_n e^{i(\omega_n t - k^* z)} \tag{14}$$

and ω_n represents the circular frequency of the nth harmonic.

2.2. The transfer function

Fig. 1 depicts a pseudo cross-section of a regolith profile, consisting of $N-1$ regolith layers deposited over a half space of bedrock. Each layer has a local coordinate system with $z_j = 0$ at the top of Layer j and increasing downwards. Assume that each of the N layers behave as a Kelvin–Voigt solid and that the regolith cross-section is vertically propagating a simple harmonic wave. In this case the wave equation in Layer j has solution of form

$$u_j(z_j,t) = B_j e^{i(\omega t + k_j^* z_j)} + C_j e^{i(\omega t - k_j^* z_j)}. \tag{15}$$

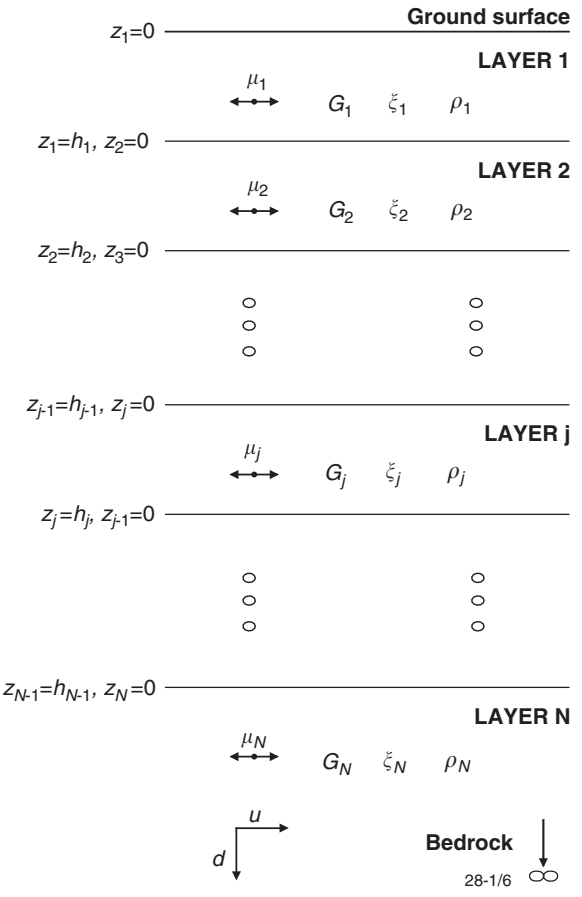

Fig. 1. Regolith cross section consisting of layers above a half space of bedrock (Layer N) where u_j, G_j, ξ_j ρ_j and h_j represent particle motion, shear modulus, damping ratio, density and thickness in (or of) Layer j respectively. Computation of transfer function relies on use of a local coordinate system for depth where $z_j = 0$ and $z_j = h_j$ at top and bottom of Layer j respectively.

The full range of harmonics are ignored at this stage since the aim is to solve the wave equation for each harmonic independently and then build the solution for all harmonics by simply summing the individual component solutions. Using Eqs. (2), (3), (7) and evaluating $\frac{\partial u(z,t)}{\partial t}$, we can express the stress, τ, in Layer j at time t and depth z_j as

$$\tau_j(z_j,t) = G^* \frac{\partial u_j(z_j,t)}{\partial z_j}. \tag{16}$$

The shear stress must equal zero at the surface as air has zero shear strength. This boundary condition is commonly known as the free surface effect and from Eqs. (16) and (15) can be expressed by

$$\tau_1(z_1 = 0,t) = \mathrm{i}k_1^* G_1^*(B_1 - C_1)\mathrm{e}^{\mathrm{i}\omega t} = 0, \tag{17}$$

which is satisfied when $B_1 = C_1$. The system must further satisfy the following two conditions across the layer boundaries:

1. Displacement at the top of Layer $j+1$ must equal the displacement at the bottom of Layer j, i.e.

$$u_{j+1}(z_{j+1} = 0,t) = u_j(z_j = h_j,t), \tag{18}$$

which reduces to

$$B_{j+1} + C_{j+1} = B_j\mathrm{e}^{\mathrm{i}k_j^* h_j} + C_j\mathrm{e}^{-\mathrm{i}k_j^* h_j}. \tag{19}$$

2. Shear stress at the top of Layer $j+1$ must equal the shear stress at the bottom of Layer j

$$\tau_{j+1}(z_{j+1} = 0,t) = \tau_j(z_j = h_j,t), \tag{20}$$

which reduces to

$$B_{j+1} - C_{j+1} = \alpha_j^*\left(B_j\mathrm{e}^{\mathrm{i}k_j^* h_j} - C_j\mathrm{e}^{-\mathrm{i}k_j^* h_j}\right). \tag{21}$$

The complex impedance ratio α_j^* is a measure of how much energy is transferred between layers j and $j+1$ and is given by

$$\alpha_j^* = \frac{k_j^* G_j^*}{k_{j+1}^* G_{j+1}^*}. \tag{22}$$

Solving Eqs. (19) and (21) simultaneously yields the recursive formulas

$$B_{j+1} = \frac{1}{2}B_j(1+\alpha_j^*)\mathrm{e}^{\mathrm{i}k_j^* h_j} + \frac{1}{2}C_j(1-\alpha_j^*)\mathrm{e}^{-\mathrm{i}k_j^* h_j} \tag{23}$$

and

$$C_{j+1} = \frac{1}{2}B_j(1-\alpha_j^*)\mathrm{e}^{\mathrm{i}k_j^* h_j} + \frac{1}{2}C_j(1+\alpha_j^*)\mathrm{e}^{-\mathrm{i}k_j^* h_j}. \tag{24}$$

Using the free surface condition $B_1 = C_1$ we can express the amplitudes B_j and C_j in terms of B_1 as follows:

$$B_j = b_j(\omega)B_1, \tag{25}$$

$$C_j = c_j(\omega)B_1, \tag{26}$$

where $b_j(\omega)$ and $c_j(\omega)$ are known as the transfer coefficients and are determined through repetitive use of the recursive Eqs. (23) and (24). The transfer coefficients relate the displacement at the top of Layer j to the displacement at the top of Layer 1 (the surface). For example; to compute B_3 in Layer 3 we would use

$$b_3(\omega) = \frac{1}{2}\left[\left(1+\alpha_1^*\alpha_2^*\right)\mathrm{e}^{\mathrm{i}(k_1^* h_1 + k_2^* h_2)} + \left(1-\alpha_1^*\alpha_2^*\right)\mathrm{e}^{\mathrm{i}(k_2^* h_2 - k_1^* h_1)}\right]. \tag{27}$$

The displacement at the top of Layer j is given by

$$u_j(z_j = 0,t) = B_j\mathrm{e}^{\mathrm{i}\omega t} + C_j\mathrm{e}^{\mathrm{i}\omega t} = \left(b_j(\omega) + c_j(\omega)\right)B_1\mathrm{e}^{\mathrm{i}\omega t}. \tag{28}$$

Using Eq. (28) we can define a transfer function $T_{ij}(\omega)$ relating the displacement at the top of Layer i to the top of Layer j as follows:

$$T_{ij}(\omega) = \frac{\left|u_i(z_i = 0,t)\right|}{\left|u_j(z_j = 0,t)\right|} = \frac{b_i(\omega) + c_i(\omega)}{b_j(\omega) + c_j(\omega)}. \tag{29}$$

If Layer i is the regolith surface layer, depicted by s , the free surface effect requires that $B_s = C_s$, implying $b_s(\omega) = c_s(\omega) = 1$ and by Eqs. (25) and (26), the transfer function becomes

$$T_{sj}(\omega) = \frac{\left|u_s(z_s = 0,t)\right|}{\left|u_j(z_j = 0,t)\right|} = \frac{2}{b_j(\omega) + c_j(\omega)}. \tag{30}$$

Table 1
Description of earthquake bedrock acceleration time histories used to determine amplification factors for Botany area

Earthquake	Date	Magnitude	Station name	Distance (km)	Component	
Coalinga	09/05/1983	Ms = 4.7	SGT (Temp)	14	350	80
Nahanni	23/12/1985	Mb = 5.4	Iverson	7	280	10
Northridge	17/01/1994	Ms = 6.6	CIT Seis. Station	41	360	90
Northridge	17/01/1994	Ms = 6.6	Mt. Wilson	45	360	90
Northridge	17/01/1994	Ms = 6.6	Pacoima Dam (Downstream)	19	175	265
San Fernando	09/02/1971	Ms = 6.6	Santa Anita Dam	27	273	3
Whittier	01/10/1987	M = 6.0	CIT Seis. Station	18	360	90

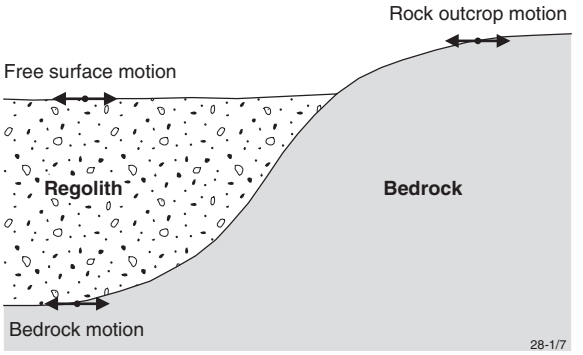

Fig. 2. Location of a rock outcrop, bedrock and free surface motion as observed from same earthquake (after Kramer, 1996).

In the Botany Bay case study, described later, earthquake accelerations measured from rock outcrops are used in the modelling process (see Table 1). The above transfer functions require a bedrock motion. Consequently, the rock outcrop motions must be converted to bedrock motions. Fig. 2 depicts the relationship between a rock outcrop, bedrock and free surface motion for the same earthquake. The conversion between rock outcrop motion and bedrock motion can be incorporated into the transfer function as follows:

$$T_{sr}(\omega)=\frac{|u_s(z_s=0,t)|}{|u_r(z_r=0,t)|}=\frac{2b_s(\omega)}{2b_r(\omega)}=\frac{1}{b_r(\omega)}, \tag{31}$$

where the subscripts r refers to the outcropping bedrock.

The transfer functions can also be used to compute amplifications in wave induced velocity and acceleration since

$$\frac{\partial u(z,t)}{\partial t}=\mathrm{i}\omega u(z,t) \tag{32}$$

and

$$\frac{\partial^2 u(z,t)}{\partial t^2}=-\omega^2 u(z,t). \tag{33}$$

Returning to the notion of multiple harmonics, it is possible to express the transfer function as follows:

$$T_{sr}(\omega_n)=\frac{1}{b_r(\omega_n)} \tag{34}$$

for the case when both layers are outcropping.

Consider a discrete acceleration time history a_r measured by an accelerometer located on outcropping bedrock. The regolith surface acceleration a_s above a layered regolith 'some' distance from the outcrop (see Fig. 2) can be computed by:

1. Computing $\hat{A}_r(\omega_n)$, the fast Fourier transform (FFT) of $a_r(t)$.
2. Calculating the transfer function $T_{sr}(\omega)$ given by Eq. (34) at all ω_n represented within $\hat{A}_r(\omega_n)$.
3. Calculating the Fourier transform of a_s as follows:

$$\hat{A}_s(\omega_n)=\hat{A}_r(\omega_n)T_{sr}(\omega_n).$$

4. Using the inverse FFT to obtain $a_s(t)$.

2.3. Strain

The time history of shear strain γ in each layer is an important input to an equivalent linear site-response analyses. Substituting Eq. (15) into Eq. (3) and differentiating yields

$$\gamma_j(z_j,t)=B_j\mathrm{i}k_j^*\mathrm{e}^{\mathrm{i}(\omega t+k_j^* z_j)}-C_j\mathrm{i}k_j^*\mathrm{e}^{\mathrm{i}(\omega t-k_j^* z_j)}, \tag{35}$$

the shear strain induced by a simple harmonic wave in Layer j. Using Eqs. (25), (26), (35) and (15) with the free surface effect we can re-write the strain in Layer j as

$$\gamma_j(z_j,t)=\frac{1}{2}\left(b_j(\omega)\mathrm{e}^{\mathrm{i}k_j^* z_j}-c_j(\omega)\mathrm{e}^{-\mathrm{i}k_j^* z_j}\right)\mathrm{i}k_j^* u_1(z_1=0,t). \tag{36}$$

Eq. (36) can be modified to compute the strain induced by a wave consisting of multiple harmonics as follows:

$$\gamma_j(z_j,t)=\sum_{n=-\infty}^{\infty}\gamma_j^{(n)}(z_j,t), \tag{37}$$

where

$$\gamma_j^{(n)}(z_j,t)=S_j(\omega_n)u_1^{(n)}(z_1=0,t). \tag{38}$$

The strain transfer function $S_j(\omega_n)$ relates the strain in Layer j to the acceleration at the surface and is given by

$$S_j(\omega_n)=\frac{1}{2}\left(b_j(\omega_n)\mathrm{e}^{\mathrm{i}k_j^* z_j}-c_j(\omega_n)\mathrm{e}^{-\mathrm{i}k_j^* z_j}\right)\mathrm{i}k_j^*. \tag{39}$$

The time history of strain in each layer for the discrete case discussed in Section 2.2 can be computed by:

1. Calculating $S_j(\omega_n)$ at a user defined depth in each layer for all ω_n represented within $\hat{A}_r(\omega_n)$. In many studies the best choice of depth is assumed to be the middle of the layer (e.g. Bardet et al., 2000).
2. Computing the FFT of strain $\hat{\gamma}$ as follows:

$$\hat{\gamma}(\omega_n)=-\frac{1}{\omega^2}S(\omega_n)\hat{A}_s(\omega_n). \tag{40}$$

3. Using the inverse FFT to obtain the strain time history $\gamma(t)$.

2.4. Equivalent linear approximation of a nonlinear response

In practice G and ξ have a functional dependence upon strain γ. Therefore, given that γ is a derivative of u

Eq. (6) is a non-linear differential equation. To solve Eq. (6) we can derive a solution to the non-linear Kelvin–Voigt wave equation (Bardet and Tobita, 2001; Joyner and Chen, 1975). The availability of geotechnical data in many broad scale studies does not justify a non-linear approach. An alternative approach involves finding the 'best' possible G and ξ and working with the linear differential equations. An equivalent linear site-response analysis estimates the 'best' possible G and ξ by using an iterative approach (Bardet et al., 2000; Idriss and Sun, 1992; Schnabel et al., 1972) and is the basis of the work described hereafter.

The ability of the equivalent linear approach to accurately capture in detail the non linear amplification associated with regolith is still under debate in the literature. EPRI (1993, Chapter 6) use experimental results to demonstrate that amplification factors derived from the equivalent linear method are similar to those derived from nonlinear models and hence use this as justification for their research with equivalent linear models. Similar results were presented by Silva et al. (1999) who illustrated favorable comparisons between equivalent linear models, nonlinear modeling and ground motion recordings. Cultera et al. (1999) use two strong motion recordings during the Northridge 1994 event to illustrate how the amplification levels predicted from an equivalent linear approach compare against physical observations. Their results indicate that one site was a close match whereas the other site's measured amplification was bounded by that modeled using an equivalent linear and a standard linear approach. Field et al. (1998), Johnson et al. (1996) and Yu et al. (1993) describe a nonlinear effect that is not accounted for by equivalent linear modelling. This effect has not been widely observed in the field however it has been linked with some unusual observations of the Northridge 1994 earthquake (Field et al., 1997). Regardless of the ongoing scientific debate, the equivalent linear approach continues to be widely used for probabilistic seismic hazard and risk analysis. Typically, the approximations inherent in such applications are considered acceptable in broad scale studies (Dhu and Jones, 2002; Toro and Silva, 2001).

Before discussing the equivalent linear site-response analysis in detail it is necessary to understand the relationships between G, ξ and γ. These relationships have been empirically determined for particular regolith classifications in the United States of America (Idriss, 1990). Typically the relationships are quantified in terms of the modulus reduction G_{red}, and damping ratio ξ, curves which relate both of these quantities to percentage strain (see Fig. 3). The modulus reduction G_{red}, is given by

$$G_{red} = \frac{G_{sec}}{G_{max}}, \tag{41}$$

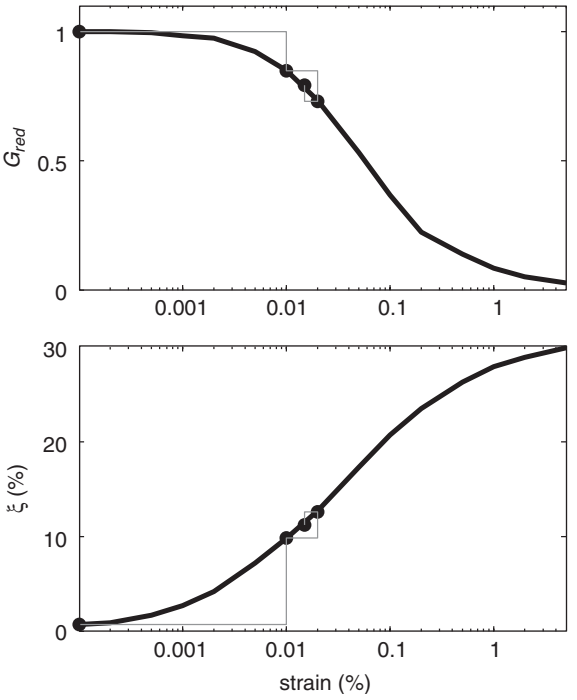

Fig. 3. Modulus reduction, G_{red} (top) and damping ratio, ξ (bottom) curves for Model Unit 1 (see Table 2). Thin lines indicate iterative convergence towards values of G_{red} and ξ that are consistent with effective strain for an example layer.

where

$$G_{max} = \rho v_s^2 \tag{42}$$

and

$$G_{sec} = \frac{\tau_c}{\gamma_c}. \tag{43}$$

Here τ_c and γ_c represent the maximum shear stress and shear strain amplitudes respectively (Kramer, 1996).

Modulus reduction and damping curves must be chosen for each of the N layers. These curves quantify how each layer is likely to perform when exposed to the propagating earthquake energy. An equivalent linear site-response analysis is performed by:

1. Assigning intitial values for G_{red} and ξ in each layer by reading in the 'first' value of their respective curves. Note that the 'first' values correspond to the smallest strain for which the curves are defined.
2. Using the assigned G_{red} and ξ to compute the strain time history as described in Section 2.3.
3. Computing the maximum strain in each layer $\gamma_j^{(max)}$ and calculating the effective shear strain in each layer using

$$\gamma_{\mathrm{j}}^{(eff)} = R_\gamma \gamma_{\mathrm{j}}^{(max)}, \tag{44}$$

where R_γ is the strain ratio. The effective strain represents a more realistic measure of the strain induced over a period of time than the maximum strain, since the maximum is only attained for a short period of time. Typically a value of 0.65 is chosen for the strain ratio, however Idriss and Sun (1992) present a method of estimating R_γ from earthquake magnitude.

4. Computing $\log_{10}\left(\gamma_j^{(eff)}\right)$ and using it to determine new values of G_{red} and ξ by linearly interpolating the modulus reduction and damping curves.
5. Comparing the percentage differences

$$\frac{100\left|G_{red}^{(i)}-G_{red}^{(i+1)}\right|}{G_{red}^{(i+1)}},\frac{100\left|G_{red}^{(i)}-G_{red}^{(i+1)}\right|}{G_{red}^{(i)}},\\ \frac{100\left|\xi^{(i+1)}-\xi^{(i)}\right|}{\xi^{(i+1)}},\frac{100\left|\xi^{(i+1)}-\xi^{(i)}\right|}{\xi^{(i)}} \quad (45)$$

to a user-defined tolerance where (i) and (i+1) refer to the previous and current iterations, respectively. If any of the percentage differences are greater than the tolerance, G_{red} and ξ are reassigned to the ($i+1$) value and the process is repeated from Step 2 using the updated G_{red} and ξ. This iterative procedure is illustrated in Fig. 3. If all of the percentages are smaller than the tolerance the updated parameters are accepted. A tolerance of around 5% is adopted by the authors and will usually lead to convergence in 3 to 4 iterations.

2.5. Response spectral acceleration and amplification factors

The response spectral acceleration describes the maximum response of a single-degree-of-freedom (SDOF) oscillator to a particular input acceleration. Buildings are often approximated by SDOF oscillators in PSHA where buildings of different height correspond to SDOF oscillators with different natural circular frequency ω_o. Response spectral acceleration is a function of the natural circular frequency (or natural period) and damping ratio of a suite of SDOF oscillators (Chopra, 2001). In practice, the damping ratio is assumed to be the same for each oscillator. Note that the response spectral acceleration does not characterise actual ground motion, rather it provides information on how SDOF oscillators respond to strong ground motion.

A periodic acceleration time history can be represented in Fourier Series by

$$a(t)=\sum_{n=-\infty}^{\infty}a_n^*e^{i\omega_n t}, \quad (46)$$

where the complex Fourier coefficients a_n^* are given by

$$a_n^*=\frac{1}{2T}\int_0^T a(t)e^{ni\pi t/t}dt. \quad (47)$$

The equation of motion for a SDOF system with mass m under load from the nth harmonic of $a(t)$ is

$$m\ddot{u}_n(t)+c\dot{u}_n(t)+ku_n(t)=-ma_n^*e^{i\omega_n t}, \quad (48)$$

where

$$c=2m\xi_b\omega_o \quad (49)$$

is the damping coefficient, ω_o the undamped natural circular frequency of the SDOF oscillator, ξ_b the SDOF damping ratio and

$$k=m\omega_o^2 \quad (50)$$

is the spring constant that characterises the elasticity of the oscillator (Kramer, 1996). The relationship between ω_o and the natural period T_o is given by

$$T_o=\frac{2\pi}{\omega_o} \quad (51)$$

The solution of Eq. (48) can be written in the form

$$u_n(t)=-H_{\omega_o}(\omega_n)a_n^*e^{i\omega_n t}, \quad (52)$$

where $H_{\omega_o}(\omega_n)$ is the transfer function relating the displacement of the SDOF oscillator to the external load. Substituting Eq. (52) into (48) and simplifying using Eqs. (49) and (50) yields

$$H_{\omega_o}(\omega_n)=\frac{1}{(\omega_o^2-\omega_n^2)+i(2\xi_b\omega_o\omega_n)}. \quad (53)$$

The response spectral acceleration associated with a given acceleration record $a(t)$, can be computed by:

1. calculating $H_{\omega_o}(\omega_n)$ for a user defined ξ_b,
2. computing the FFT of the SDOF displacement $\hat{D}_{\omega_o}(\omega_n)$ using the multiplication

$$\hat{D}_{\omega_o}(\omega_n)=H_{\omega_o}(\omega_n)\hat{A}(\omega_n), \quad (54)$$

where $\hat{A}(\omega_n)$ is the Fourier transform of the acceleration record,
3. calculating the FFT of the SDOF acceleration $\hat{A}_{\omega_o}(\omega_n)$ using

$$\hat{A}_{\omega_o}(\omega_n)=-\omega^2\hat{D}_{\omega_o}(\omega_n), \quad (55)$$

4. using the inverse FFT to compute the relative acceleration time history $a_{\omega_o}(t)$ for the SDOF oscillator with respect to the input acceleration, $a(t)$.
5. computing the total acceleration of the building

$$a_{\omega_o}^{tot}(t)=a_{\omega_o}(t)+a(t) \quad (56)$$

and finding the maximum $\max_t\left\{a_{\omega_o}^{tot}(t)\right\}$.
6. repeating steps 1–4 for a sequence of natural circular frequencies ω_o allows the construction of a response

spectral acceleration $R(\omega_o)$, where

$$R(\omega_o) = \max_t \left\{ a^{tot}_{\omega_o}(t) \right\}. \quad (57)$$

The resulting $R(\omega_o)$ categorises the maximum accelerations likely to be observed by a range of buildings exposed to the input acceleration $a(t)$.

The amplification factor F is defined as

$$F(\omega_o) = \frac{R^s(\omega_o)}{R^r(\omega_o)}, \quad (58)$$

where $R^s(\omega_o)$ is the response spectral acceleration at the regolith surface and $R^r(\omega_o)$ is the response spectral acceleration corresponding to the bedrock outcrop motion (see Fig. 2). The amplification factor is useful because it describes how the building response changes due to the propagation of a seismic wave through regolith. Typically F varies between 0.5 and 5 for different fundamental periods, bedrock motion intensities, regolith thicknesses and geotechnical properties.

Care must be taken in probabilistic seismic hazard analyses (PSHA) to ensure that only bedrock motions are used when computing or applying F. Robinson and Fulford (2005) describe how F can be applied in a PSHA by using a random earthquake generator and an attenuation model to estimate the ground motion for a suite of synthetically generated earthquakes. It is important that the attenuation models used in conjunction with F do not model site effects. Toro et al. (1997) and Atkinson and Boore (1997) provide attenuation models that do not estimate site effects.

3. Statistical simulation of models

Conducting a PSHA over a large geographical region requires classification of the area into a finite number of site classes. In this study site classes are defined as geographical regions within which the regolith is thought to be laterally homogeneous. In practice our knowledge of the geotechnical parameters in any vertical profile is uncertain due to natural variability and noise in measurements. The problem of uncertainty is increased when we extrapolate a specific profile over a large region (i.e. across a site class). O'Connor et al. (2005) demonstrated that the sensitivity of amplification factors to uncertainty in modulus reduction G_{red}, damping ratio ξ and density ρ was significantly less than the sensitivity to other key geotechnical parameters such as shear wave velocity v and layer thickness h. In this section we introduce a method for incorporating uncertainty in these key parameters when computing variability in amplification factors. The uncertainty associated with G_{red}, ξ, and ρ is omitted based on the findings of O'Connor et al. (2005).

The following two assumptions are inherent in the uncertainty analysis:

1. The soil profile can be approximated by M model units, each extending over some depth. Model units represent depth sections of similar regolith material and collectively they must cover the entire profile without overlapping. The Mth model unit is the bedrock and the first model unit starts at the surface (Fig. 4A). Note that a model unit is not the same as a

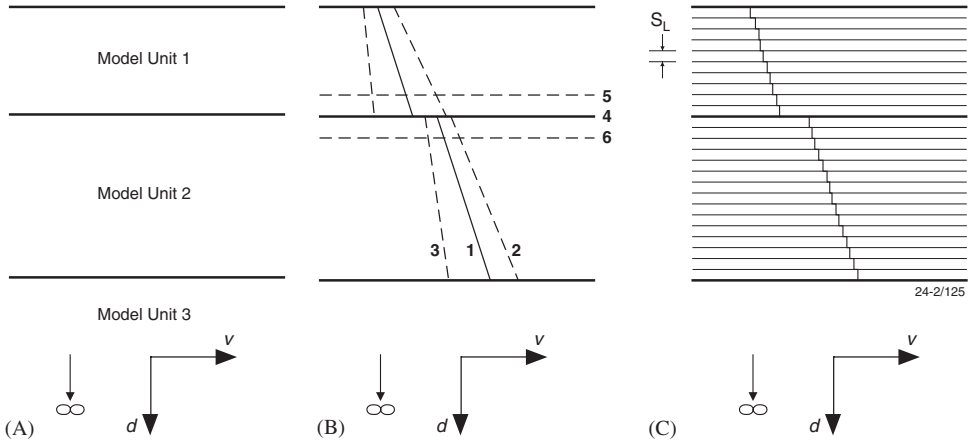

Fig. 4. Association between (A) model units, (B) linear relationship between velocity and depth and (C) computational layers in each model unit. In (B). numbered lines are defined as follows; (1) $v = \bar{m}_2 d + \bar{c}_2$, (2) $v = (\bar{m}_2 + \sigma_{m_2})d + (\bar{c}_2 + \sigma_{c_2})$, (3) $v = (\bar{m}_2 - \sigma_{m_2})d + (\bar{c}_2 - \sigma_{c_2})$, (4) $d = d_2$, (5) $d = d_2 + \sigma_{d_2}$ and (6) $d = d_2 - \sigma_{d_2}$. Symbols v and d refer to velocity and depth respectively, and m_2 and c_2 refer to slope and y-intercept of relationship between v and d in Model Unit 2. Horizontal bars above a symbol refers to mean of respective symbol and σ refers to standard deviation of subscripted symbol. In (C) thin horizontal lines indicate computational layers of thickness S_L. Vertical lines represent discretisation of line (1) from (B) and its equivalent in Model Unit 1 into computational layers.

layer, which was defined earlier for the purpose of computation. Hereafter, such layers are referred to as computational layers.
2. The velocity—depth relationship can be approximated by a linear model in each model unit (Fig. 4B).

Borehole and other geological and geophysical data are typically used to divide a study region into separate site classes. Usually there are several estimates of the depth d_j to the jth model unit in each site class. These estimates can be used to determine average depths of burial $\{\bar{d}_j\}_{j=2}^{M}$ and standard deviations $\left\{\sigma_{d_j}\right\}_{j=2}^{M}$ for each model unit.

Scatter plots of velocity versus depth can often be constructed from geotechnical data. The data within each model unit can be modelled using the line

$$v = \bar{m}_j d + \bar{c}_j, \quad z_j < d < z_{j+1} \tag{59}$$

that minimises the least squares misfit where $\bar{m}_j$ and $\bar{c}_j$ are determined from least squares analyses and d is a measure of depth from the surface (Fig. 4B). The standard deviations σ_{m_j} and σ_{c_j} associated with $\bar{m}_j$ and $\bar{c}_j$ can be computed in each model unit using the formulas of Moore and McCabe (1993) or estimated with discretion when sufficient data is not available.

The following statistics are required before the described methodology can be used to simulate regolith models:

(i) $\{\bar{m}_j\}_{j=1}^{M}$ and $\{\sigma_{m_j}\}_{j=1}^{M}$,
(ii) $\{\bar{c}_j\}_{j=1}^{M}$ and $\{\sigma_{c_j}\}_{j=1}^{M}$,
(iii) $\{\bar{d}_j\}_{j=2}^{M}$ and $\{\sigma_{d_j}\}_{j=2}^{M}$.

An interpretation of these statistics is given in Fig. 4b. It is possible to randomly generate a regolith model from these statistics by:

1. Randomly selecting the values $\{m_j\}_{j=1}^{M}$, $\{c_j\}_{j=1}^{M}$ and $\{d_j\}_{j=2}^{M}$ from the relevant normal distributions defined by the statistics in (i), (ii) and (iii) respectively.
2. Utilising a user defined layer thickness, $s_{L,}$ to divide each model unit into computational layers (Fig. 4c). These computation layers are then used to solve the wave equation as described in Section 2.
3. Computing the velocity in the middle of each layer using the relevant parameters with Eq. (59), and assigning the other parameters, e.g. ξ and G_{red} curves and ρ, based on the values assigned to the associated model unit.

Note that the number of layers assigned to each model unit depends on the depths $\{d_j\}_{j=2}^{M}$ assigned in Step 1 and the value of s_L. The depth to each model unit d_j is rounded to the nearest integer multiple of s_L. In some simulations d_j will be rounded to zero implying that a model unit will disappear altogether. This allows for the inclusion of small variable model units that cannot be regionally mapped in detail but are believed to be 'sometimes' present e.g. units such as sand lenses.

The above procedure is repeated to produce a suite of n geological profiles that are as variable (or similar) as required. Each of these profiles is used with the equivalent linear approach described in Section 2.4 to compute n estimates of the amplification factor for the site class in question. The resulting suite of amplification factors can then be used to produce estimates of uncertainty for the 'best' (or median) amplification factor.

4. Botany Bay case study

An earthquake of magnitude 6–6.5 in the Sydney region of Australia is viewed as one of the top 50 risks from natural disasters faced by the international reinsurance community (Smolka [*pers. comm.*], 2001)[1]. This perceived risk is due to the high population density, standards of building construction and the insurance exposure within Sydney. The previously described approach was used with available geotechnical information to study the potential for ground motion amplification in the Botany Bay region of Sydney. Note that the aim of this section is to provide a demonstration of our methodology and is in no way meant to be a detailed study on the earthquake hazard in Sydney.

The Botany region lies within the northern Botany Basin, which comprises a sequence of Quaternary sediments from a variety of geological environments, including beach deposits, sand dunes, tidal deltas, mud flats and swamps. In addition, man-made fills have been placed over portions of the study area. These unconsolidated deposits are often in the order of 30–35 m thick, but may be up to 70–80 m thick in places. Fig. 5 shows the four site classes that were identified around Botany using geotechnical data and seismic velocities obtained by NSW Department of Public Works and Services and Geoscience Australia. The spatial distribution of the site classes was inferred from contours of sediment thickness published by (Griffin, 1963). The properties of the sediments in each site class were constrained by the nature of the four primary sediment types identified in the Botany Basin (Roy, 1983). For more information regarding the geotechnical properties of the region and the methodologies used in estimating these properties the reader is directed to Dhu et al., (2003).

Site Class F (Fig. 6) is considered in detail in the following sections. The modulus reduction G_{red} and damping ratio ξ curves used in conjunction with Site Class F were obtained from the software package ProShake [1] (http://www.proshake.com/userman.pdf).

[1]Anselm Smolka, Munich Reinsurance Company, Germany.

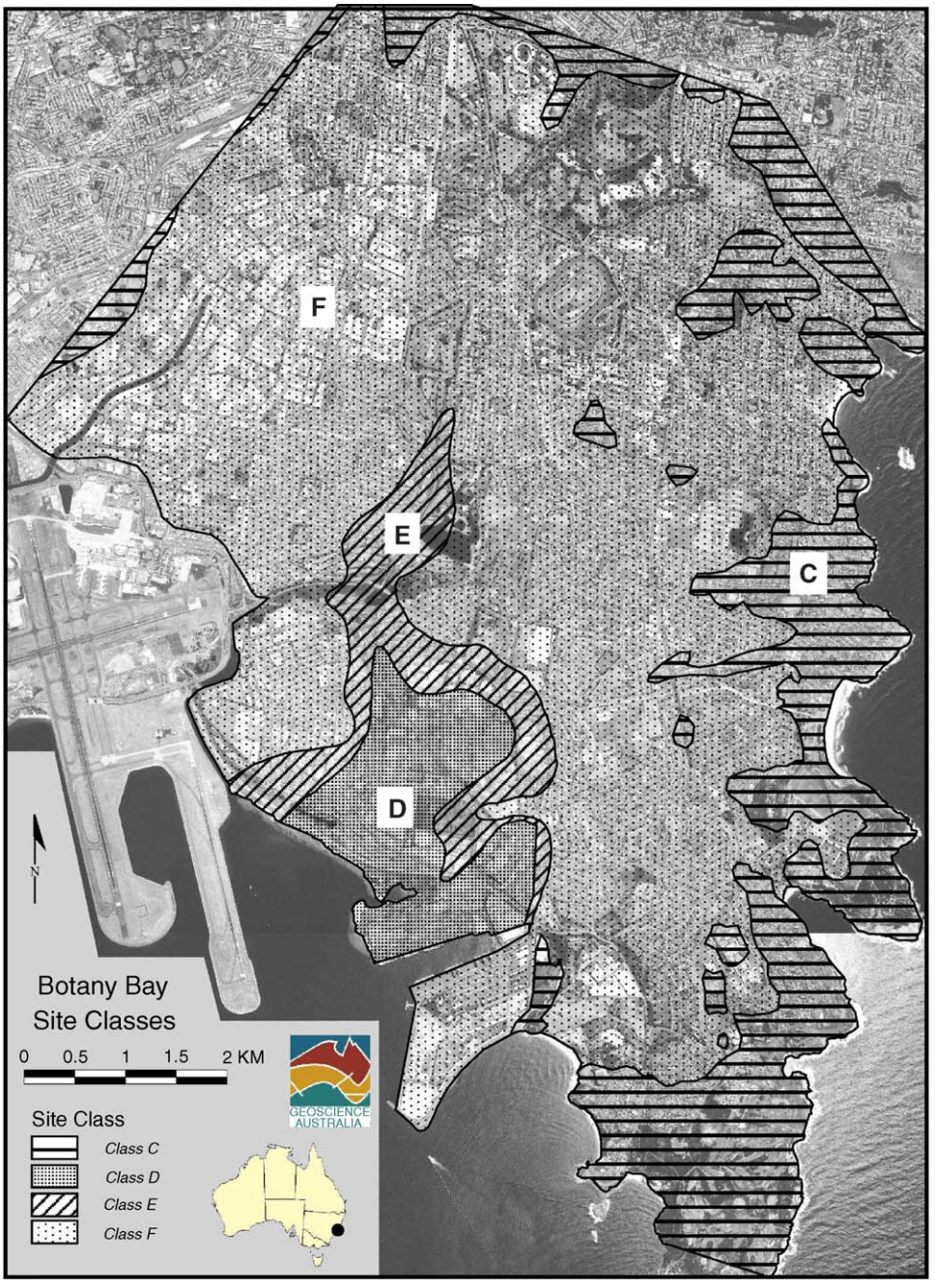

Fig. 5. Site class map for Botany Bay indicating geographical coverage of each site class.

A breakdown of the G_{red} and ξ curves by layer is given in Table 2.

4.1. Benchmarking

The suite of MATLAB programs that implement the methodology described above is collectively known as SUA and is described in the Appendix. In order to benchmark SUA we compared results for a specific example against EERA, an alternative implementation of the equivalent linear methodology (Bardet, 2000). Note that it was only possible to benchmark the outputs up to the calculation of response spectral acceleration since the computation of amplification factors and the

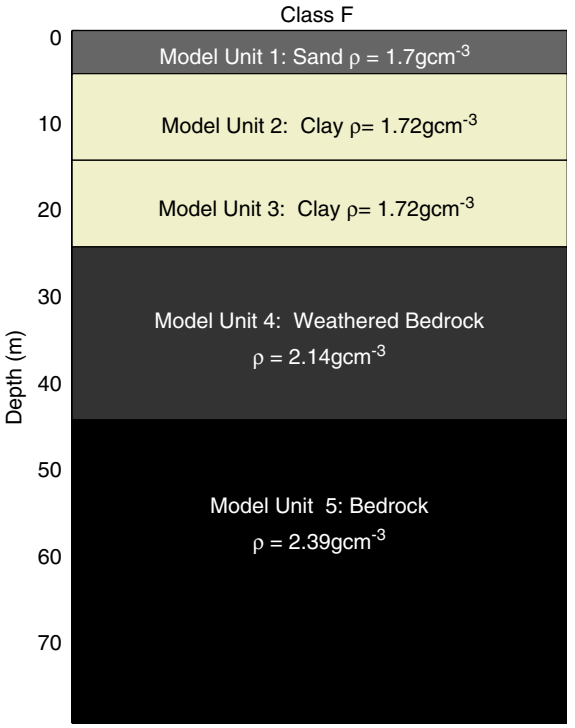

Fig. 6. Regolith cross section in Site Class *F*, a specific example of generalised case shown in Fig. 1.

Table 2
Modulus reduction G_{red} and damping ratio ξ curves associated with each model unit of Site Class *F*

Model unit	Curve	
	Modulus reduction G_{red}	Damping ratio ξ
1	Sand (Seed & Idriss)—Average	Sand (Seed & Idriss)—Average
2	Clay (Sun et al.)	Clay – PI = 20–40 (Sun et al.)
3	Clay (Sun et al.)	Clay – PI = 20–40 (Sun et al.)
4	Rock (Idriss)	Rock (Idriss)
5	Rock (Idriss)	Rock (Idriss)

Terminology is the same as that used by EduPro Civil Systems Inc. (EduPro Civil Systems, ProShake Ground Response Analysis Program, Version 1.1 User's Manual, 54pp. http://www.proshake.com/userman.pdf.).

results from the statistical simulation of models (unique to our work) are not covered in EERA. Both packages were used to compute the surface acceleration time history and the response spectral acceleration for the 10° component of the Nahanni earthquake (Table 1) and Site Class F.

Fig. 8 shows the comparison between the SUA and EERA results. No obvious difference was identified between the surface acceleration computed by either method at the scale shown in Fig. 7A. Closer inspection revealed a relative time shift of around 0.01 s (or 2 samples) which was verified using a discrete cross correlation function (Table 3). The EERA result was shifted 0.01 s to the right and the difference computed (Fig. 7B). The relative L_1, L_2 and L_∞ norms were computed to compare the difference between the SUA and EERA surface acceleration (Fig. 8). The relative L_n norm is defined by

$$L_n^{rel} = \frac{\|SUA_{SA} - EERA_{SA}\|_n}{\|EERA_{SA}\|_n}, \tag{60}$$

where SUA_{SA} and $EERA_{SA}$ are the surface acceleration computed by SUA and EERA respectively. Table 3 presents the values of each of these norms before and after the time shift. All three norms suggest a significant improvement in the comparison following correction of the time shift.

A comparison between the surface response spectral acceleration for SUA and EERA revealed a similar result up to natural periods of around 5 s, after which an oscillatory variation appears in the SUA result that is not evident in the EERA response spectral acceleration. Differences at high periods are not significant for probabilistic seismic hazard studies since most civil structures of interest exhibit natural periods less than 3 s. Overall the comparison between results is good suggesting that SUA generates comparable estimates of site-response.

4.2. Botany Bay Simulation

Fifty regolith cross sections were simulated from the Site Class F base model (Fig. 6) using the approach described in Section 2. These 50 models were used with two components of seven bedrock acceleration time histories (see Table 1) and SUA to produce amplification factors for 700 model–acceleration time history combinations. The use of 50 regolith models incorporates the uncertainty caused by variations in the regolith model. The 14 bedrock acceleration time histories were normalised to a peak ground velocity of 100 mm s^{-1} to ensure that they were symbolic of a representative earthquake with similar magnitude-distance combination. The use of multiple scaled bedrock accelerations represents a sampling of the aleatory uncertainty associated with ground motion spectral shape. The consideration of multiple earthquakes is optional; it has been included in this example to demonstrate how it can be included. Amplification factors are assumed to be log normally distributed. Note that the mean in log-space is therefore equivalent to the median in normal space. The

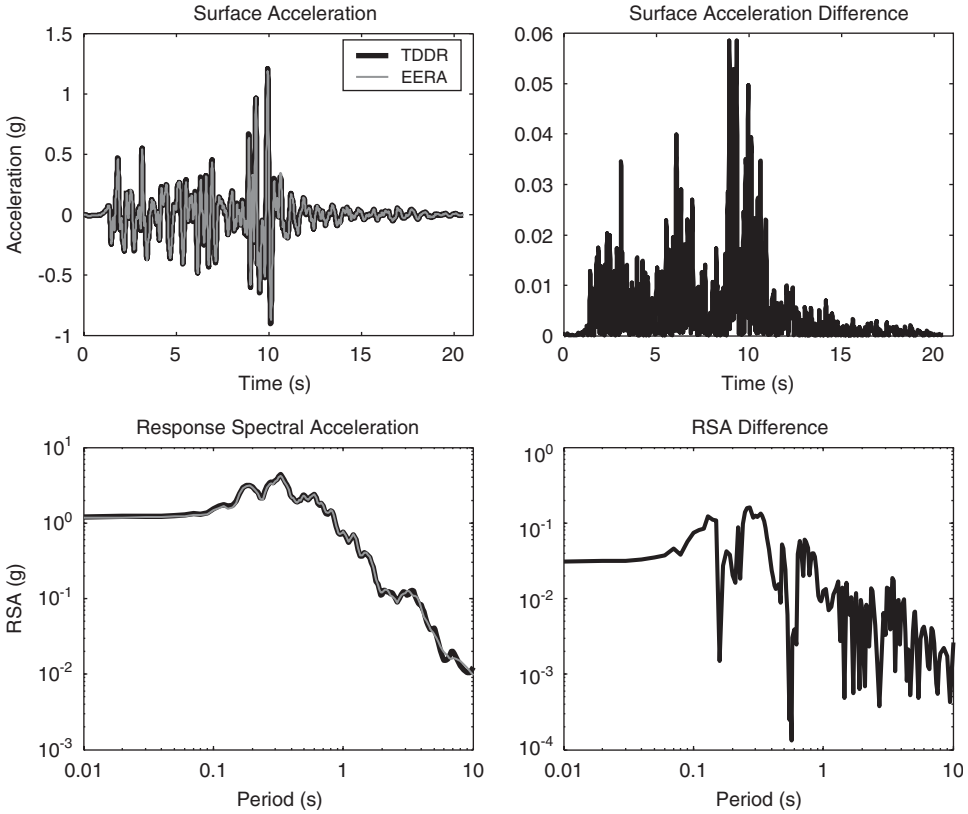

Fig. 7. Comparison between SUA and EERA results for benchmarking exercise described in Section 4.1. SUA results are drawn in a thicker font to make it easier to identify similarities.

Table 3
Results of comparison between surface acceleration computed by EERA and SUA shown before and after 0.04 s time shift

	X_{corr}	L_1^{rel}	L_2^{rel}	L_∞^{rel}
Before	128 @ 0.04 s	0.1594	0.0277	0.1624
After	128 @ 0 s	0.0591	0.0034	0.0493

Xcorr is the discrete cross-correlation function, L1rel the relative L_1 norm, L_2^{rel} the relative L_2 norm and L_∞^{rel} the relative L_∞ norm.

median amplification factor is shown with the 16th and 84th percentile in Fig. 9.

The median amplification factor indicates a maximum level of amplification of 2.8 at around 0.4 s which corresponds roughly with the natural period of one to three storey buildings. This implies that a one to three storey building located on Site Class F is expected to experience 2.8 times the horizontal acceleration experienced by the same building located on bedrock. The 84th percentile at 0.4 s indicates a 34% probability that a building will experience a level of amplification between 2.8 and 4.3 and a 16% probability that the level of amplification will exceed 4.3. The 16th percentile at 0.4 s suggests that there is an 84% probability that the amplification factor will exceed 2.

5. Conclusions

Site-response analyses are an important component of any PSHA. This paper gives a detailed description of the equivalent linear site-response methodology and provides source code, SUA to implement an equivalent linear site-response analysis. In addition, SUA implements a simple method for assessing some of the uncertainties associated with calculating site-response.

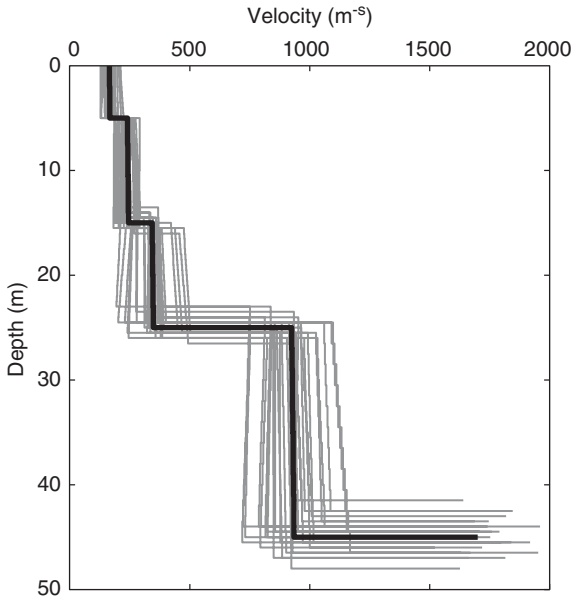

Fig. 8. Subset of geotechnical models randomly generated from Site Class F Base Model (in bold).

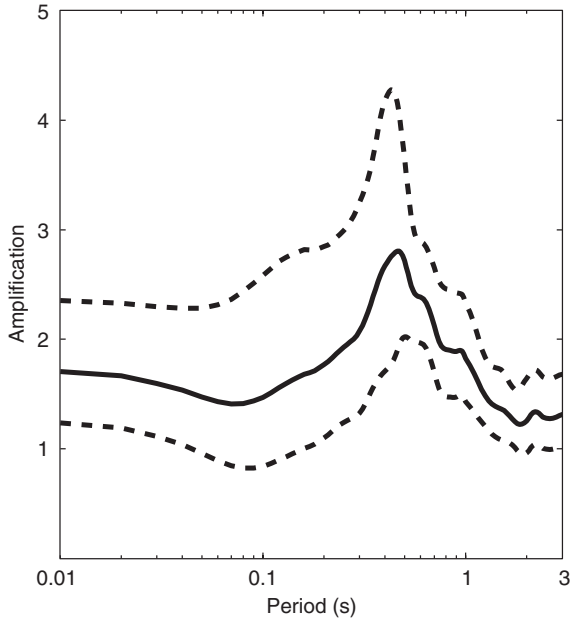

Fig. 9. Median amplification factor (solid) and 16th and 84th percentiles (dashed) for Botany Bay simulation described in Section 4.2.

The Botany Bay case study indicates that regolith can significantly amplify the ground shaking associated with an earthquake. Incorporation of uncertainty shows that a range of possible amplification factors can be expected rather than a single level of amplification. The method of assessing uncertainty presented here constitutes a relatively simplistic approach. The approach does not attempt to incorporate variability in either the damping or the modulus properties of the material, nor does it attempt to allow for variations in densities. In addition to this, the method assumes that the velocity in each regolith model unit can be represented by a linear gradient.

Whilst there are shortcomings in our incorporation of uncertainty, the simplicity of our approach affords some obvious advantages. In particular, our methodology allows a broad scale site-response analysis to be conducted even with limited geotechnical data. Furthermore, our analysis provides an indication of the level of uncertainty associated with the two geotechnical parameters, regolith thickness and seismic velocity, that the amplification factors are most sensitive too. Contrastingly, publicly available packages do not provide any measure of variability. These packages are designed for individual site-response analyses rather than attempting to define the site-response for a larger region or site class as is often required for a PSHA.

Acknowledgements

The authors would like to thank Mike Neville and Peta Anderson of the NSW Department of Public Works and Services for providing geotechnical data used in the Botany Bay case study. Walter Silva from Pacific Engineering and Analysis, California is acknowledged for ongoing collaboration in our site-response work and for assisting the authors with their understanding of site-response analyses. We would also like to thank Jean-Pierre Bardet from the University of Southern California for his helpful comments on the comparison between EERA and SUA, and Angie Jaensch, Greg Michalowski and Neil Corby from GAV at Geoscience Australia for their assistance in the production of figures for this manuscript. This paper has been greatly improved courtesy of the kind reviews provided by Phil Cummins and Matt Hayne of Geoscience Australia, as well as an anonymous reviewer.

Appendix. Subroutines in SUA

The following list describes the main subroutines in the Matlab program SUA:

TRANSFUNC is used to compute the transfer function, regolith surface acceleration and the time history of strain in each layer (see Sections 2.2 and 2.3).

EQIUVLIN is used to implement the equivalent linear approach (see Section 2.4).

RSACALC is used to compute the response spectral acceleration (see Section 2.5).

MODSIM is used to simulate the regolith models (see Section 3).

BOTANYTESTCASE demonstrates a simple site-response analysis without considering uncertainty (see Section 4.1).

BOTANYSITERESPONSEMULTI demonstrates a complete site-response analysis, including an assessment of uncertainty (see Section 4.2).

References

Annaka, T., Yashiro, H., 2000. Uncertainties in a probabilistic model for seismic hazard analysis in Japan. In: Brebbia, C.A. (Ed.), Risk Analysis II. Wessex Institute of Technology, Wessex, UK, pp. 369–378.

Atkinson, G.M., Boore, D.M., 1997. Some comparison between recent ground motion relations. Seismological Research Letters 68 (1), 94–127.

Bardet, J.P., Ichii, K., Lin, C.H., 2000. EERA: A computer program for Equivalent–linear Earthquake site Response Analyses of layered soil deposits. Department of Civil Engineering, University of Southern California, Los Angeles, California, 37pp.

Bardet, J.P., Tobita, T., 2001. NERA: A computer program for Nonlinear Earthquake site Response Analyses of layered soil deposits. Department of Civil Engineering, University of Southern California, Los Angeles, California, 43pp.

Borecherdt, R.D., Gibbs, J.F., 1976. Effects of local geologic conditions in the San Francisco Bay region on ground motions and intensities of the 1906 earthquake. Bulletin of the Seismological Society of America 66, 467–500.

Chopra, A.K., 2001. Dynamics of Structures: Theory and Applications to Earthquake Engineering. Prentice Hall, Upper Saddle River, New Jersey 844pp.

Cramer, C.H., Petersen, M.D., Reichle, M.S., 1996. A Monte Carlo approach in estimating uncertainty for a seismic hazard assessment of Los Angeles, Ventura, and Orange counties, California. Bulletin of the Seismological Society of America 86 (6), 1681–1691.

Cultera, G., Boore, D.M., Joyner, W.B., Dietel, C.M., 1999. Nonlinear soil response in the vicinity of the Van Norman Complex following the 1994 Northridge, California, Earthquake. Bulletin of the Seismological Society of America 89 (5), 1214–1231.

Dhu, T., Jones, T., 2002. Earthquake risk in Newcastle and Lake Macquarie. GA Record 2002/15, Canberra, Geoscience Australia, Australia, 271pp.

Dhu, T., Jones, T., Neville, M., 2003, Earthquake shaking susceptibility of the Botany area. GA Record, Geoscience Australia, Canberra, Australia, 23pp.

EPRI, 1993. Guidelines for determining design basis ground motions, vol. 1 Technical Report EPRI TR-102293, Electric Power Research Institute, Palo Alto, California, USA, 475pp.

EPRI, 1993. Appendices for ground motion estimation, vol 2 Guidelines for determining design basis ground motions. Technical Report EPRI TR-102293, Electric Power Research Institute, Palo Alto, California, USA, 497pp.

FEMA, 1999. Earthquake loss estimation methodology, HAZUS®99: User's Manual, ArcView® Version. Federal Emergency Management Agency, Washington DC, 316pp.

Field, E.H., Johnson, P.A., Beresnev, I.A., Zeng, Y., 1997. Nonlinear ground-motion amplification by sediments during the 1994 Northridge earthquake. Nature 390, 599–602.

Field, E.H., Kramer, S., Elgamal, A.-W., Bray, J.D., Matasovic, N., Johnson, P.A., Cramer, C., Roblee, C., Wald, D.J., Bonilla, L.F., Dimitriu, P.P., Anderson, J.G., 1998. Nonlinear site response: Where we're at (A report from a SCEC/PEER seminar and workshop). Seismological Research Letters 69 (3), 230–234.

Frankel, A.D., Mueller, C.S., Barnhard, T.P., Leyendecker, E.V., Wesson, R.L., Harmsen, S.C., Klein, F.W., Perkins, D.M., Dickman, N.C., Hanson, S.L., Hopper, M.G., 2000. USGS National seismic hazard maps. Earthquake Spectra 16 (1), 1–19.

Griffin, R.J., 1963. The Botany Basin in Bulletin of the Geological Survey NSW, Geological Survey of NSW, Sydney, Australia, 101pp.

Idriss, I.M., 1990. Response of soft soil sites during earthquakes. In: Memorial Symposium to honour Professor Harry Bolton Seed, Berkeley, California, 412pp.

Idriss, I.M., Sun, J.I., 1992. Users' manual for SHAKE91. Center for Geotechnical Modeling, Dept. of Civil and Environmental Engineering, U.C. Davis.

Iwan, W.D., 1967. On a class of models for the yielding behaviour of continuous and composite systems. Journal of Applied Mechanics 34, 612–617.

Johnson, P.A., Zinszner, B., Rasolofosaon, N.J., 1996. Resonance and elastic nonlinear phenomena in rock. Journal of Geophysical Research 101 (B5), 11,553–11,564.

Joyner, W.B., Chen, A.T.F., 1975. Calculation of nonlinear ground response in earthquakes. Bulletin of Seismological Society of America 65, 1315–1336.

Kramer, S.L., 1996. Geotechnical Earthquake Engineering. Prentice Hall, Upper Saddle River, New Jersey 653pp.

McGuire, R.K., Arabasz, W.J., 1990. An introduction to probabilistic seismic hazard analysis. In: Ward, S.H. (Ed.), Geotechnical and Environmental Geophysics, vol. III, Society of Exploration Geophysics, Tulsa, USA, pp. 333–353.

Meremonte, M., Frankel, A., Cranswick, E., Carver, D., Worley, D., 1996. Urban seismology—Northridge Aftershocks recorded by multi-scale arrays of portable digital seismographs. Bulletin of the Seismological Society of America 86 (5), 1350–1363.

Moore, D.S., McCabe, G.P., 1993. Introduction to the Practice of Statistics. second ed., W.H. Freeman and Company, New York, 854pp.

Murphy, J.R., Davis, A.H., Weavers, N.L., 1971. Amplification of seismic body waves by low-velocity surface layers. Bulletin of the Seismological Society of America 61, 109–145.

O'Connor, A., Dhu, T., Jones, A., Robinson, D., 2005. Analysis of variability in Newcastle and Lake Macquarie

regolith site response models. GA Record 2005/03, Geoscience Australia, Canberra.

Robinson, D., Fulford, G., 2005. EQRM: Geoscience Australia's Earthquake Risk Model: Technical Manual: Version 3.0, GA Record 2005/01, Geoscience Australia, Canberra.

Roy, P.S., 1983. Quaternary geology. Geology of the Sydney 1:100 000 Sheet 9130. Technical report, Geological Survey of NSW, Department of Mineral Resources, Sydney, Australia.

Schnabel, P.B., Lysmer, J., Seed, H.B., 1972. Shake: A computer program for earthquake response analysis of horizontally layered sites. Technical Report UCB/EERC-72/12, Earthquake Engineering Research Centre, University of California, Berkeley, 87pp.

Seed, H.B., Idriss, I.M., 1970. Soil moduli and damping factors for dynamic response analyses. Technical Report UCB/EERC-70/10, Earthquake Engineering Research Centre, University of California, Berkeley, 48pp.

Silva, W., 1997. Characteristics of vertical strong ground motion for applications to engineering design. In: Proceedings of the FHWA/NCEER Workshop on the National Representation of Seismic Ground Motion for New and Existing Highway Facilities, Technical Report NCEER-97-0010, National Center for Earthquake Engineering Research, Sate University of New York at Buffalo, Buffalo, New York, pp. 205–252.

Silva, W., Turcotte, W.S.T., Moriwaki, Y., 1988. Soil response to earthquake ground motion. Technical Report EPRI NP-5747, Electric Power Research Institute (EPRI), California, USA, 283pp.

Silva, W., Stokoe, K., Pyke, R., Idriss, I.M., 1999. Comparison of nonlinear and equivalent linear analyses at high strain level. Seismological Research Letters 70 (2), 217.

Stirling, M.W., Wesnousky, S.G., 1998. Probabilistic seismic hazard analysis of New Zealand. New Zealand Journal of Geology and Geophysics 41, 355–375.

Toro, G.R., Abrahamson, N.A., Schneider, J.F., 1997. Model of strong ground motions from earthquakes in Central and Eastern North America: Best estimates and uncertainties. Seismological Research Letters 68 (1), 41–57.

Toro, G.R., Silva, W.J., 2001. Scenario earthquakes for Saint Louis, MO and Memphis, TN, and seismic hazard maps for the central United States region including the effect of site conditions. Technical Report 1434-HQ-97-GR-02981, Risk Engineering, Boulder, Colorado, 248pp.

Yu, G., Anderson, J.G., Siddharthan, R., 1993. On the caharcteristics of nonlinear soil response. Bulletin of the Seismological Society of America 69 (3), 230–234.